Solar Physics (2024) 299:169
https://doi.org/10.1007/s11207-024-02401-z

REVIEW

$1/f$ Noise in the Heliosphere: A Target for PUNCH Science

Jiaming Wang[1] · William H. Matthaeus[1] · Rohit Chhiber[1,2] · Sohom Roy[1] · Rayta A. Pradata[1] · Francesco Pecora[1] · Yan Yang[1]

Received: 30 August 2024 / Accepted: 31 October 2024

Abstract

We present a broad review of $1/f$ noise observations in the heliosphere, and discuss and complement the theoretical background of generic $1/f$ models as relevant to NASA's Polarimeter to UNify the Corona and Heliosphere (PUNCH) mission. First observed in the voltage fluctuations of vacuum tubes, the scale-invariant $1/f$ spectrum has since been identified across a wide array of natural and artificial systems, including heart rate fluctuations and loudness patterns in musical compositions. In the solar wind the interplanetary magnetic field trace spectrum exhibits $1/f$ scaling within the frequency range from around 2×10^{-6} Hz to around 10^{-3} Hz at 1 au. One compelling mechanism for the generation of $1/f$ noise is the superposition principle, where a composite $1/f$ spectrum arises from the superposition of a collection of individual power-law spectra characterized by a scale-invariant distribution of correlation times. In the context of the solar wind, such a superposition could originate from scale-invariant reconnection processes in the corona. Further observations have detected $1/f$ signatures in the photosphere and corona at frequency ranges compatible with those observed at 1 au, suggesting an even lower altitude origin of $1/f$ spectrum in the solar dynamo itself. This hypothesis is bolstered by dynamo experiments and simulations that indicate inverse cascade activities, which can be linked to successive flux tube reconnections beneath the corona, and are known to generate $1/f$ noise possibly through nonlocal interactions at the largest scales. Conversely, models positing in situ generation of $1/f$ signals face causality issues in explaining the low-frequency portion of the $1/f$ spectrum. Understanding $1/f$ noise in the solar wind may inform central problems in heliospheric physics, such as the solar dynamo, coronal heating, the origin of the solar wind, and the nature of interplanetary turbulence.

1. Introduction

$1/f$ noise, otherwise known as "flicker noise", refers to a signal in which the amplitude of the spectral density $P(f)$ inversely scales with the frequency f. Such a spectrum has

Jiaming Wang (王嘉明)

✉ W.H. Matthaeus

[1] Department of Physics and Astronomy, University of Delaware, Newark, DE 19716, USA

[2] Heliophysics Science Division, NASA Goddard Space Flight Center, Greenbelt, MD 20771, USA

Published online: 23 December 2024

the unique property that the integrated power per octave remains constant across frequencies. Mathematically, the integration of the spectrum over a frequency range f_1 to f_2, i.e., $\int P(f)df \sim \int df/f \sim \log f_2/f_1$, depends solely on the ratio f_2/f_1. This total power is insensitive to rescaling of the frequency by an arbitrary factor, a reflection of the *scale invariance* of the power df/f. The distribution $P(f) \sim 1/f$ is often referred to as a scale-invariant distribution and is observed across a wide array of physical systems (see, e.g., review by Dutta and Horn 1981), including heliospheric plasmas such as the interplanetary magnetic field (Bavassano et al. 1982; Burlaga and Goldstein 1984; Matthaeus and Goldstein 1986) and elsewhere (Matthaeus et al. 2007; Bemporad, Matthaeus, and Poletto 2008). When the scale-invariant $1/f$ noise spectrum is observed, it is often fruitful to search for a scale-invariant physical process that produces the observation. In this way the study of $1/f$ noise can lead to new physical insights. Some examples of such efforts are given in Section 2.

The primitive observations of $1/f$-like solar wind magnetic field spectra (Coleman 1968; Bavassano et al. 1982; Denskat and Neubauer 1982) revealed a tendency toward spectral indices shallower than the Kolmogorov value of $-5/3$ at lower frequencies, typically below around a few times 10^{-3} Hz to a few times 10^{-5} Hz. However, the significance of $1/f$ spectrum was not fully recognized in these early reports. It was Burlaga and Goldstein (1984) who first placed an emphasis on the form f^{-1} and in addition employed data records long enough to probe frequencies down to 10^{-6} Hz and lower. The need for extended data records is a recurrent theme in identifying $1/f$ power spectrum, as discussed further in the following sections.

Understanding the origin of the interplanetary $1/f$ observations was counted among the scientific motivations for design of the Parker Solar Probe (PSP) mission (Fox et al. 2016). As will be discussed in Section 4, the interplanetary structures associated with the $1/f$ observations are necessarily very large – relevant $1/f$ spectrum begins to emerge at around 2×10^{-6} Hz and extends to around 10^{-3} Hz, corresponding to about the typical reciprocal spacecraft-frame correlation time at 1 au (Matthaeus and Goldstein 1982; Isaacs, Tessein, and Matthaeus 2015) and spanning up to more than the solar wind transit time to 1 au.

NASA's Polarimeter to UNify the Corona and Heliosphere (PUNCH) mission will likely, in principle, contain information relevant to the nature of the $1/f$ noise observed in situ. But will PUNCH be able to detect and characterize its source? At present, this is unclear, as the methods for unambiguously translating the PUNCH imagery into spectral information are still subjects of ongoing research (see Pecora et al. 2024). In anticipation of such developments, we point out this opportunity to use PUNCH to understand at some level the origin of the interplanetary $1/f$ noise. In this paper, we review a history of ideas for how $1/f$ emerges generically across various physical processes (Section 3) and make some existing and potential connections to solar wind and coronal observations. Our aim is to provide a foundational background for researchers who will mine PUNCH data for evidence concerning the origins of interplanetary $1/f$ noise.

2. Background and Examples

Low-frequency $1/f$ spectrum was first observed by Johnson (1925) when studying voltage fluctuation noise in vacuum tubes. The spectrum, such as the one shown in Figure 1, was subsequently analyzed by Schottky (1926) and termed "flicker noise". The spectrum was postulated to originate from events of foreign molecules incident upon and disrupting the electron-emitting cathodes, consequently generating voltage fluctuations with Lorentzian spectral

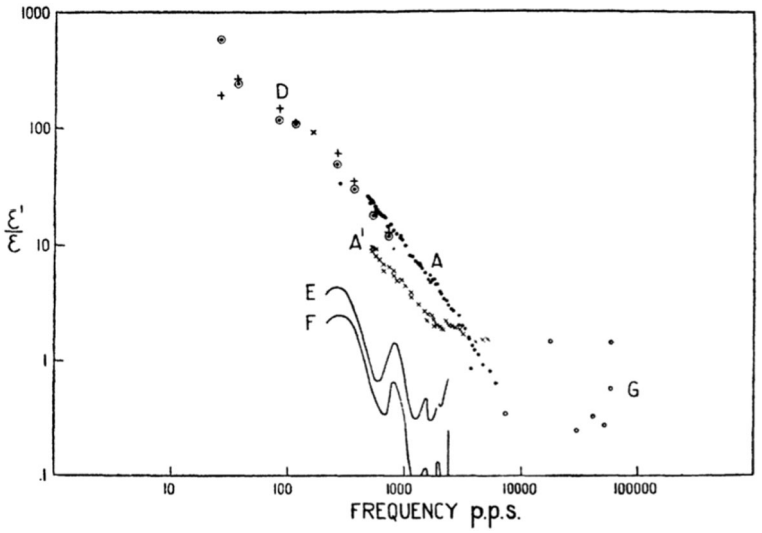

Figure 1 Spectrum of voltage fluctuations in vacuum tubes, exhibiting a range of $1/f$ scaling (Johnson 1925, Figure 6).

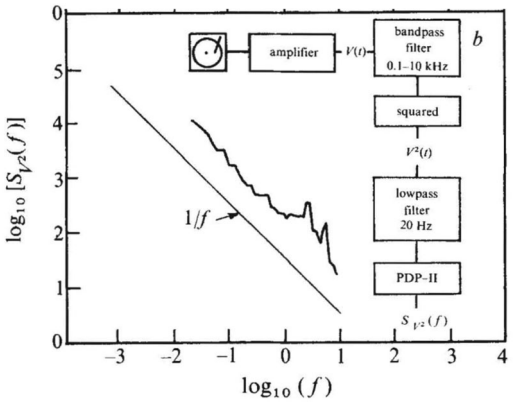

Figure 2 Spectrum of loudness fluctuations of Bach's 1st Brandenburg Concerto (Voss and Clarke 1975, Figure 1), consistent with a $1/f$ spectrum, as indicated.

profiles. Superposition of these Lorentzian profiles were later shown in many works (see, e.g., Bernamont 1937; Van Der Ziel 1950; Machlup 1981) to lead to $1/f$ spectral behavior.

Since then, $1/f$ noise has been identified and analyzed in numerous systems, including semiconductors (Van Der Ziel 1950; Caloyannides 1974), music and speech (Voss and Clarke 1975; Levitin, Chordia, and Menon 2012), human heartbeats and cognition (Kobayashi and Musha 1982; Gilden, Thornton, and Mallon 1995), and more. For instance, the distinctive $1/f$ spectrum is observed in loudness fluctuations and pitch fluctuations, such as in Bach's 1st Brandenburg Concerto (Figure 2, Voss and Clarke 1975). Other diverse examples include fluctuations in turbulent He II (Figure 3, Hoch, Busse, and Moss 1975) and in cellular automaton and other systems exhibiting self-organized criticality (Figure 4, Jensen 1990).

In the solar wind, $1/f$ spectrum is often observed to span several orders of magnitude in frequency near 1 au, extending from approximately the reciprocal of the transit time to 1 au

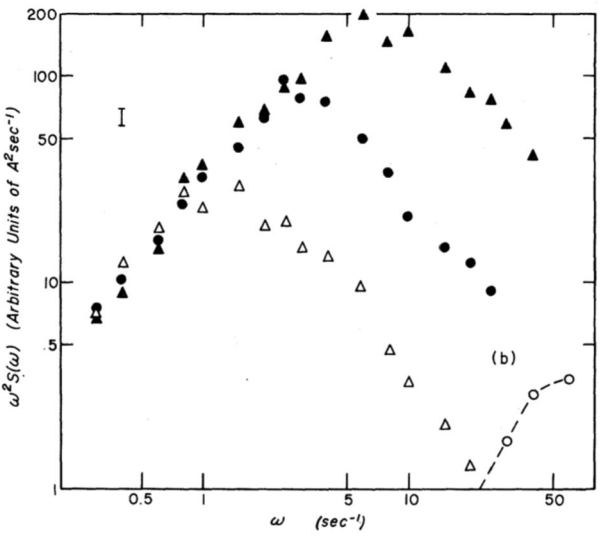

Figure 3 Spectra of noise voltage in turbulent He II exhibiting $1/\omega$ scaling below some critical frequencies, reciprocal of system's relaxation times (Hoch, Busse, and Moss 1975, Figure 4).

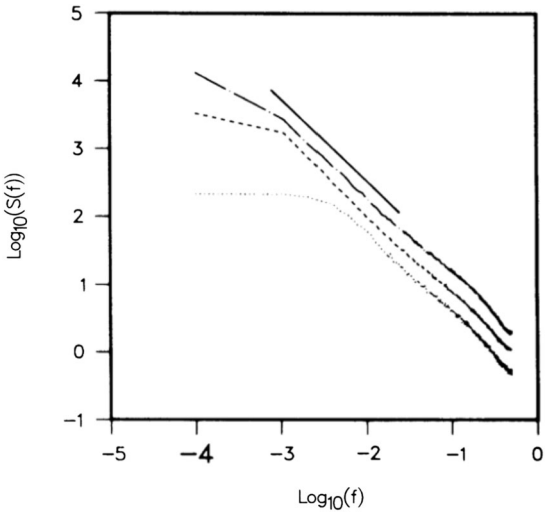

Figure 4 Spectra of total number of particles on simulated two-dimensional lattice models following simplified diffusive dynamics, exhibiting a range of $1/f$ scaling as guided by the solid line (Jensen 1990, Figure 2).

(around 100 hours) to more than two decades higher in frequency, around the reciprocal of the correlation timescale (see, e.g., Matthaeus and Goldstein 1982, 1986; Bruno and Carbone 2013). Beyond this point, the spectrum gradually transitions to the more negative "$-5/3$" or "$-3/2$" power-law indices associated with the classical descriptions of the inertial range of plasma turbulence (see, e.g., Batchelor 1970; Iroshnikov 1964; Kraichnan 1965). These classical power-law spectra are theoretically grounded in the principle of scale invariance of energy flux across scales within the inertial range, which is defined as a range of scales much smaller than a (fixed) correlation scale and much larger than a typical scale where dissipation comes into play.

One of the arguments for the generation of the $1/f$ part of the spectrum relies on a generic *superposition principle*. The principle posits that an ensemble of the so-called "purely" random signals with a scale-invariant distribution of correlation times collectively exhibits

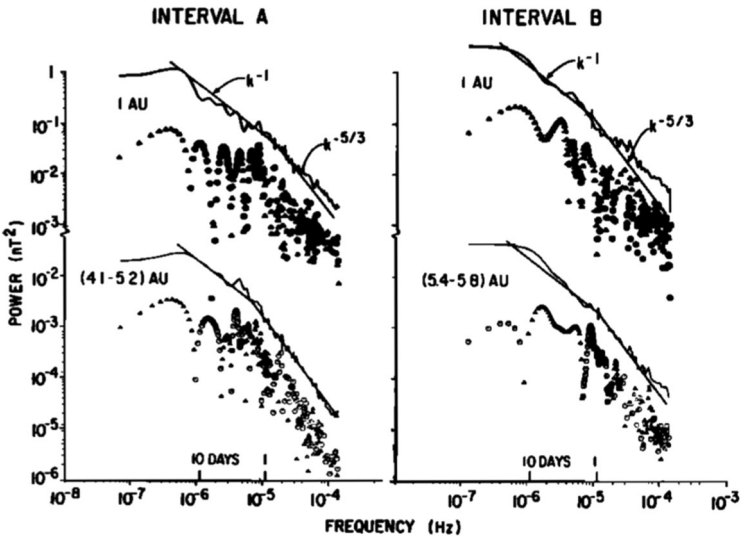

Figure 5 Magnetic field trace spectra observed at 1 au from IMP 8 and ISEE 3 and near 4 to 5 au from Voyager 1, shown as solid curves (Burlaga and Goldstein 1984, Figure 2). Triangles and circles represent positive and negative values of reduced helicity spectrum, each multiplied by frequency.

a $1/f$ spectrum (Machlup 1981, see Section 3 for details). Therefore the presence of $1/f$ signals in the solar wind can be attributed to a scenario in which the correlation scale itself is distributed in a scale-invariant fashion over a sufficiently large range of values. The possibility of a distribution of correlation scales, as opposed to a single scale, becomes relevant for complex systems, apparently including the solar wind (Ruiz et al. 2014), in which the observed fluctuations emerge from many distinct solar sources.

2.1. $1/f$ in the Solar Wind

One of the earliest observations of $1/f$ spectrum in the solar wind dates back to Bavassano et al. (1982), where it appears in the individual components of the low-frequency magnetic field spectrum near 0.3 au, as measured by the Helios 2 spacecraft. Later, Burlaga and Goldstein (1984) find $1/f$ spectrum in the trace of the magnetic field spectral tensor across more than an order of magnitude in frequency before the correlation scales, as measured at 1 au by IMP 8 and ISEE 3, as well as near 4 to 5 au by Voyager 1 (Figure 5).

Matthaeus and Goldstein (1986) observe $1/f$ noise within the frequency range of 2.7×10^{-6} to 8.5×10^{-5} Hz in the 1 au magnetic field spectrum (see Figure 6). The authors attribute it to the superposition of signals from uncorrelated magnetic reconnection events occurring in the corona near the solar surface, with their respective correlation times collectively following a log-normal distribution. This explanation relies on the general superposition principle in which the detailed properties of the individual reconnection events are not crucial (see Section 3). We should note here that the explanation of $1/f$ provided in Matthaeus and Goldstein (1986) is easily adapted to processes other than successive coronal reconnection events, or even processes occurring beneath the photosphere.

In exploring the heliocentric dependence of the magnetic field, Bruno et al. (2009) and Bruno and Carbone (2013) observe $1/f$ scaling in the trace of the magnetic spectrum in the fast solar wind at multiple distances, using data from Helios 2 (0.3 to 1 au) and Ulysses

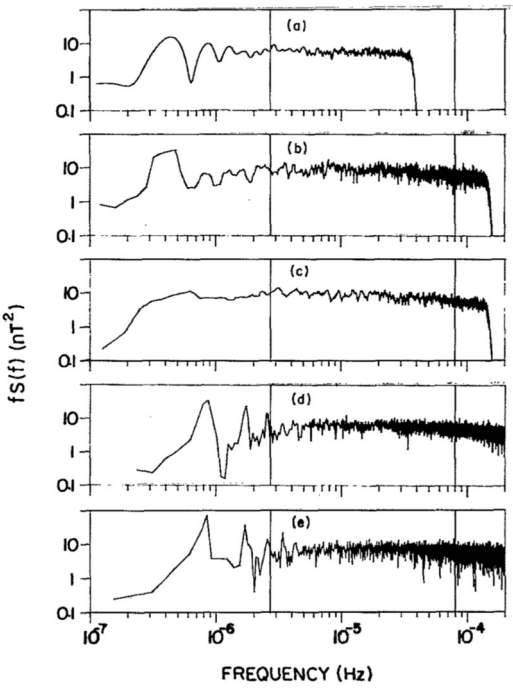

Figure 6 Compensated spectra of interplanetary magnetic field at 1 au using five intervals of data from ISEE 3 (panels a and b), IMP (panel c), and OMNI (panels d and e). $1/f$ behavior is observed between around 2×10^{-6} Hz and 10^{-4} Hz (Matthaeus and Goldstein 1986, Figure 1).

(1.4 and 4.8 au). The upper boundary of the $1/f$ range increases in frequency as heliocentric distance decreases, from approximately 10^{-4} Hz at 4.8 au to 10^{-3} Hz at 0.9 au and eventually to 10^{-2} Hz at 0.3 au. No $1/f$ signature is found in the slow wind, though it is found in a subsequent study by Bruno et al. (2019) employing long-interval data.

In a more recent study, Davis et al. (2023) analyze magnetic field measurements in the fast solar wind streams using PSP Encounter 10 measurements and observe a spectral index of -1 within the energy-containing range at distances beyond around 25 solar radii. The spectral index, however, flattens to $-1/2$ closer to the Sun (see Figure 7). The "break frequency", which serves as the approximate boundary between energy-containing and inertial scales, is also found to increase with decreasing heliocentric distance. In a companion paper, Huang et al. (2023) also analyze PSP magnetic data from Encounters 1–13, focusing specifically on intervals of solar wind with nearly constant magnetic magnitude, and find spectral indices shallower than -1 dominating the low-frequency spectrum. However, the spectral index approaches -1 with increasing wind advection time and decreasing wind speed while exhibiting no dependence on heliocentric distance. These findings suggest a dynamical and possibly radial evolution of the observed $1/f$ noise in the solar wind, which favors in situ generation mechanisms within the local wind. This type of mechanism, as opposed to the nonlocal superposition principle, could involve a linear instability or a modification to the reasoning that leads to a Kolmogorov-like cascade (Velli, Grappin, and Mangeney 1989; Verdini et al. 2012; Matteini et al. 2018; Chandran 2018). We elaborate such ideas in Section 4.

The puzzle of the origin of interplanetary $1/f$ noise presents a clear but fundamental dichotomy that is not yet unambiguously resolved – does this signal emerge from a collective statistical principle (as suggested by Matthaeus and Goldstein 1986), or is it a consequence of a particular dynamical process emerging from local dynamics alone (as suggested by

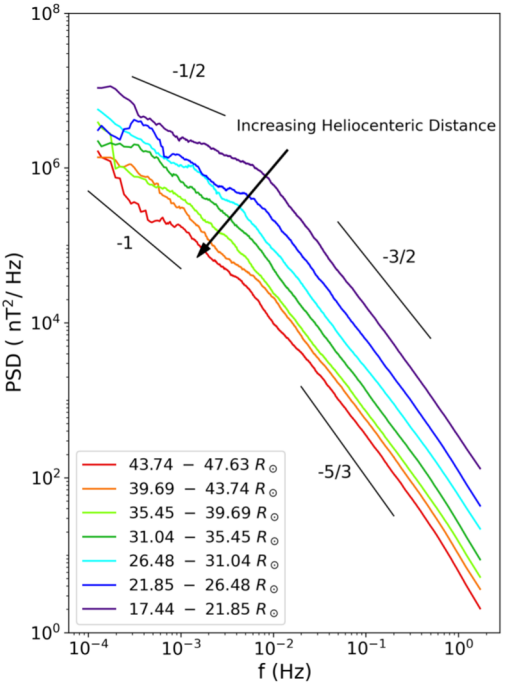

Figure 7 Magnetic field spectra of a single fast-solar-wind stream at different heliocentric distances, using data from PSP (Davis et al. 2023, Figure 3).

Davis et al. 2023; Huang et al. 2023)? In the following section, we review theories relevant to the former argument. Then in Section 4, we provide an in-depth examination of solar wind observations and related simulation and experimental results, which may shed light on this ongoing debate.

3. A Robust Superposition Principle

Theories have been established concerning a generic generation of $1/f$ noise through a superposition principle. Machlup (1981) proposes that if samples of "purely" random processes (those with autocorrelations of the form $e^{-t/\tau}$ where τ is the correlation time of the sample) exist with a minimum correlation time τ_1 and a maximum τ_2, then a scale-invariant distribution of the correlation times would lead to an averaged power spectrum exhibiting $1/f$ scaling over the frequency range $1/\tau_2 \ll \omega \ll 1/\tau_1$. The resulting $1/f$ spectrum can span several orders of magnitude if τ_2 is much greater than τ_1. However, in the context of the solar wind, two notable deviations from Machlup's model apply: (1) correlation times tend to follow log-normal distributions instead of inverse distributions (see, e.g., Ruiz et al. 2014; Isaacs, Tessein, and Matthaeus 2015), and (2) measurements typically display a Kolmogorov power-law spectrum with an index of $-5/3$ in the inertial range (on scales smaller than the correlation scales) under the regime of incompressible, isotropic magnetohydrodynamic (MHD) turbulence with high Reynolds numbers (see, e.g., Matthaeus et al. 2007; Bruno et al. 2019). Montroll and Shlesinger (1982) show that a log-normal distribution with a sufficiently large variance has an extended, inverse-like proportion. We also show in the Appendix that an ensemble of datasets with an arbitrary power-law index $-\alpha < -1$ can collectively produce a $1/f$ spectrum through the same sense of superposition.

3.1. Machlup's Superposition Principle

In examining the relationship between $1/f$ noise and its mechanism of generation, necessarily involving occurrences of unexpected or rare events,[1] Machlup (1981) hypothesizes that if the spectrum has no characteristic time – wherein the same amount of energy resides between any two frequencies separated by a fixed factor – then so might the distribution of the generating events. Suppose there exists an ensemble of nonlinear, chaotic processes naturally displaying exponentially decaying autocorrelations, and their characteristic correlation times τ follow the scale-invariant (or inverse) distribution

$$\rho(\tau)d\tau \propto \frac{d\tau}{\tau}. \tag{1}$$

Then the spectrum of an individual event, as written below in angular frequency ($\omega = 2\pi f$) domain, is of the form of a Lorentzian:

$$S(\tau, \omega) \propto \int_{-\infty}^{\infty} e^{-i\omega t} e^{-t/\tau} dt \propto \frac{\tau}{1+\omega^2\tau^2}. \tag{2}$$

The overall spectrum of this ensemble of events of equal integrated power[2] is

$$\overline{S}(\omega) = \int_{\tau_1}^{\tau_2} S(\tau, \omega)\rho(\tau)d\tau \propto \frac{\tan^{-1}(\tau\omega)}{\omega}\Big|_{\tau_1}^{\tau_2}, \tag{3}$$

where τ_1 and τ_2 are the minimum and maximum correlation times of the generating events, respectively. If the correlation times span several orders of magnitudes, i.e., $\tau_1 \ll \tau_2$, then within the frequency region satisfying $\tau_1 \ll 1/\omega \ll \tau_2$,

$$\overline{S}(\omega) \propto \frac{\pi/2 + \mathcal{O}(\tau_2\omega)^{-1} + \mathcal{O}(\tau_1\omega)^1}{\omega}. \tag{4}$$

To a zeroth-order approximation, $\overline{S}(\omega) \propto 1/\omega$.

3.2. Connection Between Inverse and Log-Normal Distributions

We note that the correlation time distribution as given in Eq. 1 is not integrable, neither are the sharp boundaries of τ_1 and τ_2 assumed in the last section physical. So what exactly happens in the limits as $\tau \to 0$ and $\tau \to \infty$? Montroll and Shlesinger (1982) propose the log-normal distribution that behaves like $1/\tau$ in the intermediate range and naturally governs multiplicative processes in which the total probability is the product of probabilities of several independent random variables.

A log-normal distribution describes a random variable X whose logarithm is normally distributed. Suppose Z is a standard normal variable. Then a log-normal distribution is defined for variable $X = e^{\mu+\sigma Z}$ as

$$f(x) = \frac{1}{x\sigma\sqrt{2\pi}} \exp\left[-\frac{(\log x - \mu)^2}{2\sigma^2}\right], \tag{5}$$

[1] Events with scale-invariant occurrences are often considered unexpected because the tail of the distribution is asymptotic and nonintegrable. So tail events are inherently rare but always possible, making them unexpected.

[2] Derivation of Machlup (1981) assumes that all samples in the ensemble share the same variance, or integrated power across scales. However, this condition is not necessary – $1/f$ spectrum can still emerge following the logic of Eq. 3 if the variances follow a scale-invariant distribution.

where μ and σ is the mean and standard deviation of the variable $\log X$, respectively. From Eq. 5, an inverse scaling $f(x) \sim 1/x$ under certain conditions becomes apparent. If we define $\overline{x} \equiv e^{\mu}$, then $f(x) \propto 1/x$ when

$$\frac{\left[\log(x/\overline{x})\right]^2}{2\sigma^2} \ll 1. \tag{6}$$

Following conventions from Montroll and Shlesinger (1982), given a fraction of tolerable deviation θ, a log-normal distribution is scale-invariant within a fraction of θ inside the domain of random variable x satisfying[3]

$$\left|\log\left(\frac{x}{\overline{x}}\right)\right| \leq \sqrt{2\theta\sigma^2}. \tag{7}$$

It is known that many solar wind variables, such as the correlation times, solar wind speed, density, temperature, magnetic field strength, and so on, follow log-normal distributions (see, e.g., Burlaga and Szabo 1999; Padhye, Smith, and Matthaeus 2001; Ruiz et al. 2014; Isaacs, Tessein, and Matthaeus 2015).[4] The abundance of log-normal distributions may be attributed to the multiplicative nature of physical processes occurring within the solar wind. Suppose the value of a random variable X is based on the product of N independent variables $X_1, \ldots, X_N$, i.e.,

$$X = X_1 \times \cdots \times X_N. \tag{8}$$

Then evoking the Lyapunov central limit theorem, the distribution of the logarithm, $\log X = \log X_1 + \cdots + \log X_N$, follows a normal distribution if certain regular conditions are satisfied. In Shockley (1957), X may represent the productivity of a researcher, whereas $X_{1,\ldots,N}$ represent research merits, such as the ability to recognize a research topic, the ability to evaluate results, and so on.

In the case of the solar wind, $X_{1,\ldots,N}$ may represent successive reconnection events or successive foldings in a dynamo (see, e.g., Matthaeus and Goldstein 1986; Bourgoin et al. 2002; Ponty, Politano, and Pinton 2004; Dmitruk and Matthaeus 2007). In particular, magnetic structures of initial lengthscale λ_0 may experience N successive reconnections, each modifying λ_0 by a factor of $(1+\epsilon)$, so that the ensemble lengthscale $\lambda = \lambda_0(1+\epsilon)^N$ mimics Eq. 8 and is log-normally distributed (Matthaeus and Goldstein 1986). In such cases where the successive events $X_{1,\ldots,N}$ are identical, the Lindeberg–Lévy central limit theorem dictates that $\log X$ is normally distributed for sufficiently large N if the second moment of $\log X_{1,\ldots,N}$ exists.

4. Theoretical Issues and Further Observations

The superposition principle elaborated upon in Section 3 provides a compact pathway to explain the generation of $1/f$ signals, but it is not specific regarding the origin of the underlying processes that are superposed. Therefore any hypothesis concerning the nature of

[3]The condition in Montroll and Shlesinger (1982) is $|\log(x/\overline{x})| \leq 2\theta\sigma^2$, which is established in log scale. The condition as in Eq. 7 is established in linear scale.

[4]We note that a detailed analysis by Feynman and Ruzmaikin (1994) finds potential departure from log-normality in hourly averaged magnetic fluctuations at 1 au. However, the distribution of 3-hour averaged magnetic magnitudes is found to be close to log-normal. A recent study by Huang et al. (2024a) employing PSP data reports that after removing power-law radial dependence, intervals of magnetic magnitudes displaying Gaussianity permeate the Alfvénic solar wind.

these processes must be assessed for consistency based on principles beyond the superposition mechanism itself. On this basis, the suggestion by Matthaeus and Goldstein (1986) that the superposition involves successive reconnections occurring in the deep corona avoids problems related to the available time scales. Specifically, sub-Alfvénic coronal dynamics (including reconnections) are not strongly limited by convection time or expansion time, since in this region the MHD characteristics travel both toward and away from the Sun.

While there has been a variety of mechanisms proposed to explain shallow $1/f$ solar wind spectra, especially in the trace magnetic field component spectra, these mechanisms are usefully categorized into those that operate *locally* in the interplanetary medium and those that originate in the lower corona or even in the solar interior. From a practical and physical point of view, the region for local processes can be viewed as the super-Alfvénic solar wind, whereas coronal and solar processes operate at lower altitudes. We distinguish local and solar mechanisms for generating the $1/f$ signal in this simple and perhaps ad hoc way.

4.1. Local Origins of $1/f$

The pioneering observations by Burlaga and Goldstein (1984) set the stage for wide ranging investigations into the origins of the interplanetary $1/f$ signal. It is worth noting that their Figure 2 (Figure 5 here) is labeled by both frequency and wavenumber, where the wavenumber spectrum assumes the form k^{-1}, in accordance with the Taylor frozen-in hypothesis (Taylor 1938).

Associated with this spectral law, Burlaga and Goldstein (1984) offered as a possible explanation for the observed $1/f$ an inverse cascade of magnetic helicity. We evaluate this as a suggestion of a local process. (We revisit it later as a possible solar process.) The inverse cascade process operates in the regime of incompressible magnetohydrodynamics (MHD; see Frisch et al. 1975; Montgomery, Turner, and Vahala 1978) under conditions where helicity is an ideal invariant. In freely decaying turbulence with appropriate boundary conditions, magnetic helicity is known to be important and can be responsible for effects such as Taylor relaxation (Taylor 1974) or selective decay (Montgomery, Turner, and Vahala 1979). Although these mechanisms are intriguing and physically appealing, their applicability to the solar wind is questionable, as the magnetic helicity of fluctuations is not an ideal invariant in magnetohydrodynamics (MHD) when a mean field is present – such as the Parker spiral field that threads the interplanetary medium. In addition, inverse cascade processes are generally very slow compared to direct cascade processes, and the observed $1/f$ range at 1 au has only a few nonlinear times to develop during transit from the Sun (Zhou et al. 1990). In any case the inverse cascade scenario involves *local* MHD scale processes that would need to occur in transit from the corona if the process is to be considered local.

On the other hand, the case where $1/f$ signal is already present below the Alfvén critical region is unrelated to in situ solar wind dynamics and avoids transit time issues. Burlaga and Goldstein (1984) mention the possibility of an alternative explanation that would involve "some appropriate superposition of streams". This suggestion was subsequently developed into the Matthaeus and Goldstein (1986) model, which employed the superposition principle described in Section 3.

Another theoretical approach to explaining the solar wind's $1/f$ spectrum as a local process was proposed by Velli, Grappin, and Mangeney (1989) and Verdini et al. (2012). Their model differs from the superposition principle in that the physical processes producing the $1/f$ signal occur in situ in the evolving solar wind due to the interaction of Kolmogorov-like nonlinear effects and the influence of expansion. Ideas along these lines have been

examined in recent Parker Solar Probe (PSP) observations (Davis et al. 2023; Huang et al. 2023), though remote generation in the corona is not ruled out by these authors. A variant of the above ideas has appeared in a recent preprint (Huang et al. 2024b).

These recent studies based on PSP observations discuss their results in the context of the models proposed by Chandran (2018) and Matteini et al. (2018). Chandran (2018) uses weak-turbulence theory to suggest that the $1/f$ behavior can arise from the parametric decay of Alfvén waves that are initially highly imbalanced (with a dominant outward propagating mode), leading to an inverse cascade wherein the dominant Alfvén mode acquires a $1/f$ scaling over time. A narrowing of the range of frequencies displaying $1/f$ is then predicted for heliocentric distances smaller than 0.3 au. A similar prediction was made by Matteini et al. (2018) based on arguments relating to the low magnetic compressibility of the solar wind. The authors conjecture that $1/f$ is the steepest possible spectrum at (large) scales where $\delta B/B \sim 1$, a limit imposed by the saturation of magnetic fluctuations δB that are bounded on a sphere of radius equal to the background field B. Consequently, near the Sun, where $\delta B/B < 1$ (see, e.g., Chhiber 2022), the $1/f$ range is predicted to disappear. See Huang et al. (2023) for a detailed discussion on how models by Chandran (2018) and Matteini et al. (2018) are used to interpret recent PSP observations.

4.2. Causality and Range of Influence

A feature of all the local mechanisms presented so far is that they refer only to observed frequencies above around 10^{-4} Hz (see, e.g., Huang et al. 2023; Davis et al. 2023). However, as emphasized above, the entirety of the observed interplanetary $1/f$ signal extends to frequencies as low as 2×10^{-6} Hz.[5] Huang et al. (2023) and Davis et al. (2023) study the tendency toward slopes shallower than the inertial range values, and even shallower than $1/f$, when examining frequencies between 10^{-2} and 10^{-4} Hz, a phenomena noted in similar frequency ranges in early works (Bavassano et al. 1982; Denskat and Neubauer 1982) without clear explanation. Without prejudice to the applicability of the local mechanisms down to 10^{-4} Hz, we may ask if such processes can be extended to much lower frequencies. Nearly two more decades of frequency must be accessed to include the full observed $1/f$ range.

The concept of causality or "range of influence" becomes critical at this juncture (Zhou et al. 1990; Chhiber 2018; Matthaeus et al. 2018). We ask the question: Over what distance can MHD processes exert influence during passage to 1 au? An estimation of this distance amounts to a position-dependent estimate of an MHD causality limit using a few key time and space scales. Start by assessing the maximum distance an MHD signal can travel in transit to 1 au $= 1.5 \times 10^{13}$ cm. The transit time for the wind at 400 km/s is then $T_{\rm tr} \sim 3.8 \times 10^5$ s. An upper bound estimate of range of influence using the Alfvén speed (~ 50 km/s) is $L_{\rm roi} = V_A T_{\rm tr} \sim 0.1$ au. This corresponds to a time of passage $T_{\rm roi} = L_{\rm roi}/V_{\rm SW} \approx 3.5 \times 10^4$ s and a frequency $f_{\rm roi} = 1/T_{\rm roi} = 2.8 \times 10^{-5}$ Hz. This is the lowest frequency that can be influenced by Alfvén wave propagation at 1 au. For turbulent motions propagating at speed $\delta V < V_A$, the range of influence will decrease, and the corresponding frequency will be higher than $f_{\rm roi}$. The fiducial line drawn in Figure 6 is around 8×10^{-5} Hz and in the present estimation would correspond to a turbulence amplitude a factor of 2 or 3 smaller than V_A.

The range of influence can be meaningfully compared with other time and length scales. First, the correlation scale L_c at 1 au is on average around 10^6 km, with broad variation (Ruiz

[5] In fact, it is possible that the signal extends to even lower frequencies. However, the signal tends to merge with harmonics of the solar rotation period, as seen in Figure 6.

et al. 2014). At $V_{SW} = 400\,\mathrm{km/s}$, a structure of size L_c passes an observation point in $2.5 \times 10^3\,\mathrm{s}$, corresponding to $4 \times 10^{-4}\,\mathrm{Hz}$, again with substantial variation. This is comfortably greater than the frequency associated with range of influence, as it must be.

Next, we note that solar wind plasma streaming transits 1 au at 400 km/s in time $T_{tr} \sim 100\,\mathrm{hr}$, or in frequency, $f_{tr} = 1/T_{tr} \sim 2.8 \times 10^{-6}\,\mathrm{Hz}$. Comparing these with observations (e.g., Figure 6), we see that the $1/f$ noise range rather neatly spans (and extends somewhat beyond) the frequency interval from f_{tr} to f_{roi}.

The fact that the nominal correlation frequency is somewhat higher than the range of influence frequency is reasonable and expected. The spectrum is well known to roll over into $\sim f^{-5/3}$ at frequencies above f_{cor}. However, since the correlation lengths in individual samples are known to be log-normally distributed (Ruiz et al. 2014), this rollover is not expected to be sharp. Moreover, as stated above, the range of influence differs in turbulence with different amplitudes δV, and this amplitude itself is broadly distributed, perhaps again in a log-normal fashion (Padhye, Smith, and Matthaeus 2001). Finally, the approximation that the log-normal distribution of correlation times is nearly scale-invariant may break down at the extremes of the $1/f$ spectral range. Given these variabilities, it seems inevitable that the transition from the $1/f$ range to the turbulence $f^{-5/3}$ range takes place gradually. In observations such as Figures 5, 6, and 7, this transition takes place over about a decade of frequency.

Consideration of the above timescale inequalities implies that a Kolmogorov-like direct cascade, or any process requiring standard nonlinear turbulence time scales, will not be able to operate over the full range of the observed $1/f$ spectrum in the time of available transit to 1 au. Analogous estimates can be readily made for other heliocentric distances or other values of turbulence timescales. This casts doubt on theoretical explanations for the $1/f$ signals. Minimally it indicates that in situ explanations must be supplemented by some other nonlocal process that fortuitously produces a spectrum that smoothly matches the spectrum that extends to much lower frequencies.

4.3. Origin in Coronal and Solar Processes

In conjunction with $1/f$ observations from long data records at 1 au, Matthaeus and Goldstein (1986) offered a theoretical explanation based on a particular scenario in which the Montroll–Shlesinger–Machlup superposition principle (see Section 3) is invoked. It is based on the elementary idea that a collision between two flux tubes can lead to reconnection and merging, producing a plasmoid with a larger cross-section, potentially doubling in size if the colliding flux tubes are of equal dimensions. This process is repeatable given a certain probability for reconnection and merger. Several stages of such merger lead to a multiplicative process and hierarchy that may be described using a log-normal distribution. Then, invoking the developments of Montroll and Shlesinger (1982), a scale-invariant distribution can be achieved over some range of scale sizes. As these structures are accelerated into the solar wind, they plausibly represent the $1/f$ signal observed without further dynamical evolution. The model of Mullan (1990) based on photospheric and coronal observations added considerable detail to the successive, scale-invariant coronal reconnection model. A cartoon taken from Mullan (1990) is shown here as Figure 8.

The concept that coronal reconnection is a multiscale process capable of supporting numerous successive reconnections is well founded in observations, based on the detection of the low-lying mixed polarity magnetic carpet (Schrijver and Title 2003). Simulations have shown that prolific flux tube collisions and resulting current sheet formation are to be expected in this highly dynamic, anisotropic turbulent medium (see, e.g., Einaudi and Velli 1994; Servidio et al. 2009).

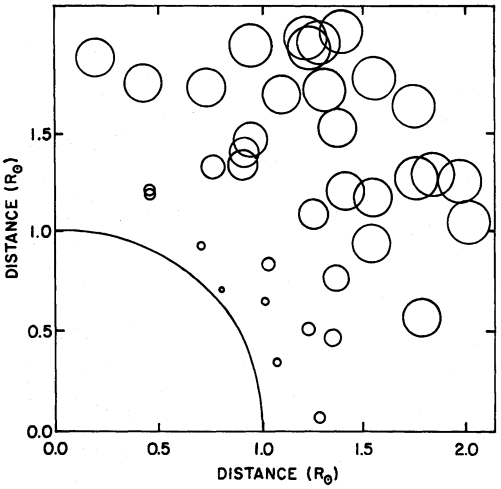

Figure 8 Cartoon of successive scale-invariant reconnection model as interpreted by Mullan (1990).

The successive reconnection scenario readily lends itself to a description of a multiplicative process in the sense of Eq. 8. The expectation of a log-normal distribution of the resulting correlation scales follows immediately, and in fact, such a distribution is observed (see, e.g., Ruiz et al. 2014; Isaacs, Tessein, and Matthaeus 2015).

Another mechanism operating in the corona has been suggested by Magyar and Van Doorsselaere (2022), based on the coupling of Alfvén waves with a transversely inhomogeneous background density field. Through 3D compressible MHD simulations, in which transverse velocity perturbations are injected at the lower boundary, the authors demonstrate that the resulting magnetic field line oscillations exhibit coherent behavior, leading to the formation of transverse collective modes, such as surface Alfvén waves. This occurs when the coupling between the waves and the inhomogeneous background is fully considered. Under linear processes like phase mixing and resonant absorption, these surface Alfvén waves develop a perpendicular energy spectrum that mirrors that of the background density. As a result, an inhomogeneous density field with a perpendicular $1/f$ spectrum can give rise to a $1/f$ spectrum in the perpendicular Alfvén velocity fluctuations. However, the authors acknowledge that the spectral index of density field in the solar corona remains uncertain, with values reported to range from -1 to -2 (Woo and Armstrong 1979; Moncuquet et al. 2020; Carley et al. 2021). Additionally, it is unclear how this process relates to the photospheric magnetic structure and features of the solar dynamo, as we discuss in Section 5.

4.4. Spectral Evolution and Generation of Correlation

The above scenario is essentially a coronal process that does not require the participation of in situ dynamics in the super-Alfvénic wind. However, as the solar wind expands, local turbulence can generate spatial correlations in the form of the Kolmogorov spectrum and its hierarchy of *locally produced* magnetic field and vorticity structures (Bruno and Carbone 2013). A familiar and often quoted *net* product of such nonlinear couplings is a net flux of energy through the inertial range toward smaller scales. However, this *cascade* is the average result of a vast number of triadic interactions (Verma 2019), which transfer energy almost equally toward larger and smaller scales, with the net being toward the latter.

This property has numerous influences on a turbulent system, but relevant here is the expectation that freely evolving turbulence will generate correlations at increasing scales.

This is a fundamental feature of the de Karman and Howarth (1938) analysis of homogeneous turbulence, and it implies that the similarity scale that defines the long-wavelength bound on the inertial range must increase in time. In the present context, this leads to the observed increase in length scale of the solar wind correlations on average with increasing radial distance (Klein et al. 1992; Ruiz et al. 2014). This gradually converts the observed high frequency part of the $1/f$ range into the correlated Kolmogorov-like $f^{-5/3}$ (or $k^{-5/3}$ using the frozen-in property) range. Indeed, this is observed and well documented (Tu and Marsch 1995; Bruno and Carbone 2013) as the upper end of the $1/f$ range evolves toward lower frequency at increasing radial distance. This has been often described as the migration toward lower frequency of the "break point" between the Kolmogorov and $1/f$ spectral ranges (Bavassano et al. 1982; Tu, Pu, and Wei 1984; Tu and Marsch 1995; Wu et al. 2020, 2021), even if this transition is often gradual rather than sharp, as illustrated, e.g., in Figure 7.

5. Connections to Inverse Cascade and Dynamo

The possibility that the observed $1/f$ signal is related to inverse cascade (Frisch et al. 1975; Fyfe, Montgomery, and Joyce 1977) activity crucially depends on where the process is purported to occur. For in situ inverse cascade-related activity in the super-Alfvénic solar wind, the issue of available time immediately enters. The problem with establishing the observed $1/f$ spectrum in the interplanetary medium due to direct cascade processes was discussed in Section 4.2. However, it is well known that inverse cascade processes are significantly slower than their direct cascade counterparts and have been been shown in various circumstances to require many, even hundreds, of nonlinear eddy turnover times to have significant effects (Dmitruk and Matthaeus 2007; Dmitruk et al. 2011) on low-frequency time variations. On this basis, it seems that accounting for the full frequency range of the observed $1/f$ solar wind noise through inverse cascade in the super-Alfvénic solar wind is essentially ruled out.

In the sub-Alfvénic corona and in the solar dynamo, the situation regarding inverse cascade activity is markedly different. In the low plasma-beta corona, plasma turbulence is likely characterized by a high degree of quasi-two dimensional anisotropy, often described by *Reduced Magnetohydrodynamics* (RMHD; Kadomtsev and Pogutse 1974; Rappazzo et al. 2008; Gómez, Martín, and Dmitruk 2013; Perez and Chandran 2013). Such systems asymptotically approach two dimensionality, a limit in which a *quasi-conserved* mean square magnetic potential can apparently support inverse cascade activity (Fyfe, Montgomery, and Joyce 1977; Dmitruk and Matthaeus 2007). This process is indeed associated with successive reconnections of a sea of magnetic flux tubes (Servidio et al. 2010). It is also associated with the more rapid decay of energy relative to mean square potential (Matthaeus and Montgomery 1980), a feature known as *selective decay*. Therefore it is possible to view the model for $1/f$ driven by scale-invariant coronal reconnections (Matthaeus and Goldstein 1986; Mullan 1990) as supported by inverse cascade processes.

Likewise, for the solar dynamo, connections between inverse cascade and $1/f$ noise generation are equally clear. Observations provide a "smoking gun" involvement of subphotospheric dynamics in producing observable spectral signatures. Particularly suggestive are observed azimuthal wavenumber spectra from photospheric line-of-sight magnetic fields reported by Nakagawa and Levine (1974) using Kitt Peak magnetograms and by Matthaeus et al. (2007) employing data from the SOHO/MDI instrument. In each case, there is evidence of a $1/k$ dependence in the photospheric *spatial* structure, which may be regarded as a signature of MHD inverse cascade (Frisch et al. 1975). Elementary models provide a

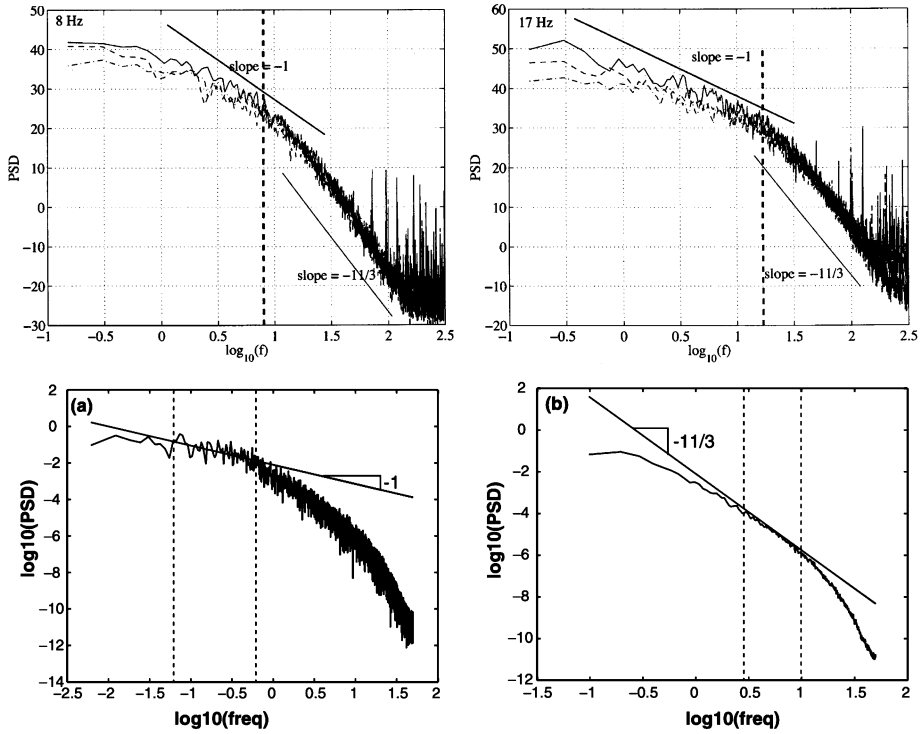

Figure 9 Top: Frequency spectra of magnetic field from liquid sodium dynamo experiment with low (left panel) and high (right panel) disk rotation rate (Bourgoin et al. 2002, Figure 11). Bottom: Magnetic spectra from low magnetic Prandtl number and large kinetic Reynolds number simulation estimated over long (left panel) and short (right panel) intervals. $1/f$ appears in frequency domain between $1/t_0$ to $1/(10t_0)$ where t_0 is the magnetic diffusion timescale (Ponty, Politano, and Pinton 2004, Figure 4).

simple relationship between spatial structures in the photosphere and observed spectra in the solar wind (Giacalone, Jokipii, and Matthaeus 2006).

On the theoretical side, spherical MHD dynamo simulations carried out for very long time scales indicate spectral transfer consistent with inverse cascade while also producing $1/f$ noise in the time domain. Such simulations employ highly idealized boundary conditions and ideal MHD equations (Dmitruk et al. 2014), thus enabling long timescale runs. The $1/f$ signals appear when runs are initialized with significant magnetic helicity or with significant rotation. In the same instances, the flows experience strong condensation of energy into the largest scale degrees of freedom in the sphere, a signature of the possibility of inverse cascade (as in Frisch et al. 1975). There is also support for dynamo generation of $1/f$ in laboratory experiments (Bourgoin et al. 2002; Gailitis et al. 2004) and supporting simulations (see Ponty, Politano, and Pinton 2004; Ponty et al. 2005, and Figure 9).

6. Observability by PUNCH

Remarkably, and perhaps fortuitously, the PUNCH mission (Deforest et al. 2022) will provide images covering a range of scales arguably of direct relevance to the observed $1/f$

spectra. PUNCH's high-resolution imaging data is designed to have at least $10\times$ better resolution than previous imagers such as STEREO (DeForest et al. 2016, 2018), thus in principle resolving structures at scales within the turbulence inertial range. Roughly speaking, PUNCH images will span scales up to a few 1 au, and with resolutions as fine as 10^6 km, comparable to the expected correlation scale. Therefore PUNCH will in principle capture images of the plasma responsible for the $1/f$ signal. The challenge lies in the interpretation of the images.

One issue is that PUNCH will detect density variations, not magnetic field, except perhaps by inference with regards to coronal structures (see, e.g., DeForest et al. 2016, 2018; Ruffolo et al. 2020). However, there are some in situ observations of $1/f$ signal in density (Matthaeus et al. 2007), as well as inferred results from the SOHO UVCS instrument in the deep corona (Bemporad, Matthaeus, and Poletto 2008). PUNCH will also observe the inner solar wind and corona in a different orientation than either STEREO imaging, or in situ measurements such as those from the ACE or Wind missions at a fixed position using the Taylor hypothesis. Figure 10 illustrates the essence of these differences in a highly idealized format. The most significant issue in quantifying the correspondence between PUNCH images and spectral characteristics is the averaging over depth of field that is intrinsic in PUNCH images. This greatly complicates the interpretation of image spatial scales to the in situ observed range of $1/f$ frequencies.

Preliminary studies of this problem have begun in anticipation of the PUNCH launch (see Pecora et al. 2024). Efforts so far have adopted a constructive procedure in which data from magnetohydrodynamic numerical simulations of turbulence are subject to modeling to in effect synthesize PUNCH data. This takes into account not only the line-of-sight integration, but also the three-dimensional response due to Thomson scattering of white light from the heliospheric density variations. Progress in these studies have shown that standard turbulence spectral scalings are modified in the synthetic PUNCH images, even if there are promising indications that information about the original properties of the turbulent field remains present. Such studies are first steps in understanding whether PUNCH will allow quantitative diagnosis of the presence of the low-frequency $1/f$ signals. Provided that ongoing studies can establish useful connections between PUNCH images and spectral distributions, this mission will have the potential to reveal the origin and evolution of the elusive interplanetary $1/f$ signal.

7. Discussion

$1/f$ noise appears in such a wide variety of physical systems (Dutta and Horn 1981) that it is difficult to fully review its occurrences in a limited space. Nevertheless, we attempt here to provide a broad but incomplete survey to suggest its generic nature. There are also a variety of detailed mechanisms that are suggested to explain its emergence. We have not delved deeply into these in systems other than the heliosphere, favoring instead a *class of models* based on the classical developments due to Van Der Ziel (1950) and Machlup (1981) and extended by Montroll and Shlesinger (1982). The basic idea is that an ensemble with a scale-invariant distribution of relaxation times, when superposed and sampled, gives rise to a range of $1/f$ behavior. The applicability of this reasoning is substantially extended upon the realization (Montroll and Shlesinger 1982) that a log-normal distribution of relaxation times can readily produce the range of scale-invariant relaxation times required to obtain $1/f$ spectrum. We presented arguments and reviewed observations that provide evidence leading us to favor the above *scale-invariant superposition* explanation. We should note,

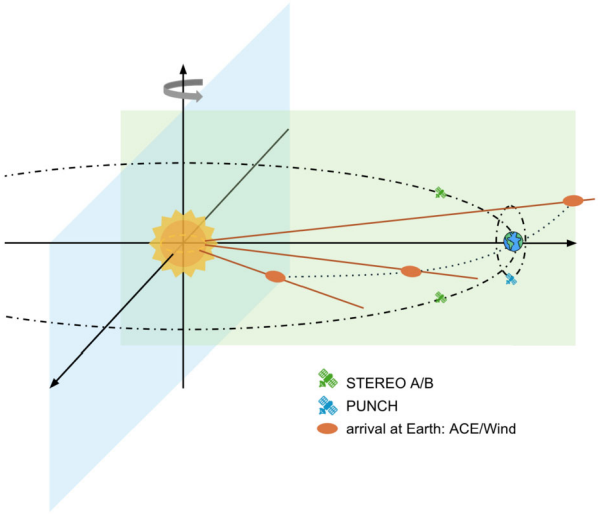

Figure 10 Projected fields of view (FOV) of STEREO A/B (green plane) and PUNCH (blue plane), both perpendicular to the ecliptic plane. Wind parcels that have reached or will reach Earth as observed by ACE/Wind are labeled in orange, with the simple assumption that the solar wind corotates rigidly with the Sun.

once again, that our review is not exhaustive and that statistical explanations such as *self-organized criticality* have been offered as a variant explanation (Bak, Tang, and Wiesenfeld 1987).

For heliospheric $1/f$ noise, we reviewed two distinct models: a coronal model based on successive reconnections manifestly related to the superposition principle and another model that relies on the generation of $1/f$ due to inverse cascade in the solar dynamo. The latter model may also fit the superposition class if the underlying mechanism (not reviewed here) involves successive stretch-and-fold dynamics (Vaĭnshteĭn and Zel'dovich 1972; Rincon 2019).

Both of the above models are intrinsically nonlinear, and neither appears to be limited by available time for developing dynamics. This is not the case for models originating in the super-Alfvénic wind, where available time is limited by convection time to the position of observation. We have explained how this limited range of influence disallows inverse cascade to very long wavelengths and also limits the ability of any MHD process to access the low frequencies ($\sim 10^{-6}$ Hz at which $1/f$ is observed at 1 au). This is not to say that local mechanisms proposed to explain $1/f$-like spectra near 10^{-4} Hz need to be rejected (Velli, Grappin, and Mangeney 1989; Chandran 2018; Davis et al. 2023; Huang et al. 2023); it does provide a challenge to explain how the local $1/f$ spectrum matches smoothly onto the $1/f$ signal that extends to near 10^{-6} Hz. In this regard, it is useful to recall the adage from Machlup (1981): *"If you have not found the* $1/f$ *spectrum, it is because you have not waited long enough."*

Because long data records are needed to study the $1/f$ signal, there have been relatively few in depth studies of its origins and connections to solar or coronal phenomena. The purpose of the present paper has been to assemble an overview of current knowledge about $1/f$ in the heliosphere and to point toward what we believe are the likely close connections between the solar dynamo, coronal dynamics, and effects observed in the super-Alfvénic wind, including 1 au and beyond. As the space physics community delves into these likely connections, the possibility may emerge that deeper knowledge of $1/f$ noise and relevant statistics might translate into quantitative connections to solar terrestrial relations and, perhaps eventually, connections to space weather prediction. At present, this is a speculative remark, and we might even imagine that modulation of $1/f$ noise might be a trigger for

rare events such as large flares or CMEs. If such connections are established, then it could represent an entirely new and statistical approach to this complex coupling between solar dynamics and geospace responses.

Although observations and simulations are continuing to reveal aspects of $1/f$ noise in the heliosphere, it is fair to say that there remain aspects and many details that are incompletely understood. We anticipate that advanced instrumentation on upcoming missions such as PUNCH will provide valuable information to further reveal the mysteries of phenomena such as $1/f$ noise in the solar wind.

Appendix: $1/f$ from Arbitrary Spectral Index

In this appendix, we build upon the discussion in Section 3.1 to demonstrate that the superposition-based generation mechanism for $1/f$ noise is applicable to a time series ensemble with any index $-\alpha$, where $\alpha > 1$. A straightforward approach (Matthaeus and Goldstein 1986) is to assume, in place of the Lorentzian profile in Eq. 2, the following form for individual time series' spectrum:

$$S(\tau, \omega) \propto \frac{\tau}{(1+\omega^2\tau^2)^{\alpha/2}}, \tag{A1}$$

where $S(\omega)$ is flat at small frequencies ($\omega\tau \ll 1$) and has a power-law index of $-\alpha$ at large frequencies ($\omega\tau \gg 1$). With inversely distributed correlation times as in Eq. 1, the superposed spectrum becomes

$$\begin{aligned}\overline{S}(\omega) &\propto \frac{1}{\omega}\int_{x_1}^{x_2}\frac{dx}{(1+x^2)^{\alpha/2}} \\ &= \frac{1}{\omega}\left[\int_0^{\infty}\frac{dx}{(1+x^2)^{\alpha/2}} - \int_0^{x_1}\frac{dx}{(1+x^2)^{\alpha/2}} - \int_{x_2}^{\infty}\frac{dx}{(1+x^2)^{\alpha/2}}\right],\end{aligned} \tag{A2}$$

where $x \equiv \omega\tau$, and in the frequency range of interest, $x_1 \equiv \omega\tau_1 \ll 1$ and $x_2 \equiv \omega\tau_2 \gg 1$. The first integral in Eq. A2 has a definite solution of $\sqrt{\pi}\Gamma[(\alpha-1)/2]/2\Gamma(\alpha/2)$, where Γ denotes the gamma function. The third integral can be approximated as $\int_{x_2}^{\infty} dx/x^{\alpha} = x_2^{1-\alpha}/(\alpha - 1)$ for $x_2 \gg 1$. The solution to the second integral is proportional to the hypergeometric function, $x_{12}F_1(1/2, \alpha/2; 3/2; -x_1^2) = x_1 - \alpha x_1^3/6 + \mathcal{O}(x_1^5)$. Thus

$$\overline{S}(\omega) \propto \frac{1}{\omega}\left[\frac{\sqrt{\pi}\Gamma(\frac{\alpha-1}{2})}{2\Gamma(\frac{\alpha}{2})} - \mathcal{O}(x_2^{1-\alpha}) - x_1 + \mathcal{O}(x_1^3)\right]. \tag{A3}$$

To the least order approximation, $\overline{S}(\omega) \propto 1/\omega$ only if $\alpha > 1$, that is, the order of the second term in the bracket is less than that of the first term. The constraint of $\alpha > 1$ also ensures that $\Gamma[(\alpha-1)/2]$ is positive.

We now propose an alternative derivation of $1/f$ noise that avoids the hypergeometric function (as well as other complicated math) and avoids assuming a certain spectral form, as in Eq. A1. Instead, we assume that the spectrum is flat below a certain break frequency and transitions to a power-law at higher frequencies. The main idea is to evaluate the expected slope of $\log(\overline{S})(\log(\omega))$ through assigning a weighting function for the slopes at any given ω. To maintain clarity in notation, we now use τ_c to represent the correlation time for an individual time series. The associated frequency, at which the power spectrum transitions

from a flat profile to a power-law decay with an index of $-\alpha$, is denoted as $\omega_c \equiv 1/\tau_c$. Meanwhile, ω indicates the range of frequencies within the domain of interest.

The reciprocal of an inversely distributed random variable is also inversely distributed. Indeed, ω_c follows the distribution

$$\rho(\omega_c)d\omega_c = \frac{d\omega_c}{\omega_c \log(\omega_1/\omega_2)}, \tag{A4}$$

where $\omega_1 \equiv 1/\tau_1 > \omega_2 \equiv 1/\tau_2$, and $\omega_c \in [\omega_2, \omega_1]$. For each power density spectrum normalized to an equal total power (of unity for example), the height of the power spectral density at ω_c is denoted as S_c and is constant at lower frequencies. The values of S_c are inversely proportional to ω_c and are inversely distributed as

$$\rho(S_c)dS_c = \frac{dS_c}{S_c \log(\omega_1/\omega_2)}. \tag{A5}$$

Above the break frequency, a power spectrum follows the form $S(\omega) = S_c(\omega/\omega_c)^{-\alpha}$ assuming continuity. Therefore, at any given frequency ω, the power-law index, denoted as β, is either 0 if the chosen spectrum has $\omega_c > \omega$ or $-\alpha$ if $\omega_c < \omega$. Intuitively, the expected value of β is

$$\overline{\beta}(\omega) = \frac{\int_{S_c(\omega_1)}^{S_c(\omega_2)} \beta(\omega) S(\omega) \rho(S_c) dS_c}{\int_{S_c(\omega_1)}^{S_c(\omega_2)} S(\omega)\rho(S_c)dS_c}, \tag{A6}$$

where $S_c(\omega)$ represents the magnitude S_c given the spectrum has a break frequency at ω. Here $\rho(S_c)$ can be considered as the probability density of $S(\omega)$, and $S(\omega)$ is the weighting function of β at frequency ω.

Why is $S(\omega)$ the weighting function of $\beta(\omega)$ under the context of spectrum superposition? To show this, consider two spectra $S_\mu(\omega) \propto (\omega/\omega_\mu)^\mu$ and $S_\nu(\omega) \propto (\omega/\omega_\nu)^\nu$ of power-law indices μ and ν, respectively, where ω_μ and ω_ν are arbitrary positive constants. The slope of $S_\mu + S_\nu$ in log-log scale can be directly calculated as

$$\frac{\partial}{\partial \log(\omega)} \log(S_\mu + S_\nu) = \frac{d\omega}{d\log(\omega)} \frac{\partial}{\partial \omega} \log(S_\mu + S_\nu) = \frac{\mu S_\mu + \nu S_\nu}{S_\mu + S_\nu}. \tag{A7}$$

We have shown that on log-log scale, power indices of power spectra can be computed with a weighted average.

The expectation $\overline{\beta}(\omega)$ can now be confidently computed using Eq. A6, keeping in mind that $\beta = -\alpha$ when $S_c > S(\omega)$ and $\beta = 0$ otherwise:

$$\begin{aligned}\overline{\beta}(\omega) &= \frac{-\alpha \int_{S_c(\omega)}^{S_c(\omega_2)} S_c(\omega/\omega_c)^{-\alpha} \rho(S_c) dS_c}{\int_{S_c(\omega_1)}^{S_c(\omega)} S_c \rho(S_c) dS_c + \int_{S_c(\omega)}^{S_c(\omega_2)} S_c(\omega/\omega_c)^{-\alpha}\rho(S_c)dS_c} \\ &= -\alpha \left[1 + (1-\alpha)\frac{1-(\omega/\omega_1)}{(\omega_2/\omega)^{\alpha-1} - 1}\right]^{-1}. \end{aligned} \tag{A8}$$

Within the frequency region where $\omega_2 \ll \omega \ll \omega_1$, assuming that $\alpha > 1$, we arrive at the desired result of $\overline{\beta}(\omega) = -1$.

Acknowledgments This research is partially supported by the NASA LWS grants 80NSSC20K0377 (subcontract 655-001) and 80NSSC22K1020, by the NASA IMAP project at UD under subcontract SUB0000317 from Princeton University, by the NASA/SWRI PUNCH subcontract N99054DS at the University of Delaware, by the NASA HSR grant 80NSSC18K1648, and by National Science Foundation grant AGS-2108834.

Author contributions J.W. contributed writing, figures, bibliography, analyses, original work in Appendix, proofreading. W.M. contributed writing, bibliography and coordination of contributions. R.C. contributed to writing several sections, proofreading. S.R. contributed to critique of overall structure, checking calculations, and proofreading. R. P. contributed to supporting analyses. F.P. contributed to connection to PUNCH mission. Y.Y. contributed to connections to PUNCH mission, proofreading.

Data Availability No datasets were generated or analysed during the current study.

Declarations

Competing interests The authors declare no competing interests.

References

Bak, P., Tang, C., Wiesenfeld, K.: 1987, *Phys. Rev. Lett.* **59**, 381. DOI.
Batchelor, G.K.: 1970, *The Theory of Homogeneous Turbulence*, Cambridge University Press, Cambridge.
Bavassano, B., Dobrowolny, M., Mariani, F., Ness, N.F.: 1982, *J. Geophys. Res.* **87**, 3617. DOI.
Bemporad, A., Matthaeus, W.H., Poletto, G.: 2008, *Astrophys. J. Lett.* **677**, L137. DOI.
Bernamont, J.: 1937, *Proc. Phys. Soc.* **49**, 138. DOI.
Bourgoin, M., Marié, L., Pétrélis, F., et al.: 2002, *Phys. Fluids* **14**, 3046. DOI.
Bruno, R., Carbone, V.: 2013, *Living Rev. Solar Phys.* **10**, 2. DOI.
Bruno, R., Carbone, V., Vörös, Z., et al.: 2009, *Earth Moon Planets* **104**, 101. DOI.
Bruno, R., Telloni, D., Sorriso-Valvo, L., et al.: 2019, *Astron. Astrophys.* **627**, A96. DOI.
Burlaga, L.F., Goldstein, M.L.: 1984, *J. Geophys. Res.* **89**, 6813. DOI.
Burlaga, L.F., Szabo, A.: 1999, *Space Sci. Rev.* **87**, 137. DOI.
Caloyannides, M.A.: 1974, *J. Appl. Phys.* **45**, 307. DOI.
Carley, E.P., Cecconi, B., Reid, H.A., et al.: 2021, *Astrophys. J.* **921**, 3. DOI.
Chandran, B.D.G.: 2018, *J. Plasma Phys.* **84**, 905840106. DOI.
Chhiber, R.: 2018 PhD thesis, University of Delaware.
Chhiber, R.: 2022, *Astrophys. J.* **939**, 33. DOI.
Coleman, P.J.: 1968, *Astrophys. J.* **153**, 371. DOI.
Davis, N., Chandran, B.D.G., Bowen, T.A., et al.: 2023, *Astrophys. J.* **950**, 154. DOI.
de Karman, T., Howarth, L.: 1938, *Proc. Roy. So. London Ser. A* **164**, 192. DOI.
DeForest, C.E., Matthaeus, W.H., Viall, N.M., Cranmer, S.R.: 2016, *Astrophys. J.* **828**, 66. DOI.
DeForest, C.E., Howard, R.A., Velli, M., Viall, N., Vourlidas, A.: 2018, *Astrophys. J.* **862**, 18. DOI.
Deforest, C., Killough, R., Gibson, S., et al.: 2022 In: *2022 IEEE Aerospace Conference*, 1. DOI.
Denskat, K.U., Neubauer, F.M.: 1982, *J. Geophys. Res.* **87**, 2215. DOI.
Dmitruk, P., Matthaeus, W.H.: 2007, *Phys. Rev. E* **76**, 036305. DOI.
Dmitruk, P., Mininni, P.D., Pouquet, A., Servidio, S., Matthaeus, W.H.: 2011, *Phys. Rev. E* **83**, 066318. DOI.
Dmitruk, P., Mininni, P.D., Pouquet, A., Servidio, S., Matthaeus, W.H.: 2014, *Phys. Rev. E* **90**, 043010. DOI.
Dutta, P., Horn, P.M.: 1981, *Rev. Mod. Phys.* **53**, 497. DOI.
Einaudi, G., Velli, M.: 1994, *Space Sci. Rev.* **68**, 97. DOI.

Feynman, J., Ruzmaikin, A.: 1994, *J. Geophys. Res.* **99**, 17645. DOI.
Fox, N.J., Velli, M.C., Bale, S.D., et al.: 2016, *Space Sci. Rev.* **204**, 7. DOI.
Frisch, U., Pouquet, A., Leorat, J., Mazure, A.: 1975, *J. Fluid Mech.* **68**, 769. DOI.
Fyfe, D., Montgomery, D., Joyce, G.: 1977, *J. Plasma Phys.* **17**, 369. DOI.
Gailitis, A., Lielausis, O., Platacis, E., Gerbeth, G., Stefani, F.: 2004, *Phys. Plasmas* **11**, 2838. DOI.
Giacalone, J., Jokipii, J.R., Matthaeus, W.H.: 2006, *Astrophys. J. Lett.* **641**, L61. DOI.
Gilden, D.L., Thornton, T., Mallon, M.W.: 1995, *Science* **267**, 1837. DOI.
Gómez, D., Martín, L.N., Dmitruk, P.: 2013, *Adv. Space Res.* **51**, 1916. DOI.
Hoch, H., Busse, L., Moss, F.: 1975, *Phys. Rev. Lett.* **34**, 384. DOI.
Huang, Z., Velli, M., Shi, C., et al.: 2024b. e-prints, arXiv, DOI.
Huang, Z., Sioulas, N., Shi, C., et al.: 2023, *Astrophys. J. Lett.* **950**, L8. DOI.
Huang, Z., Shi, C., Velli, M., et al.: 2024a, *Astrophys. J. Lett.* **973**, L26. DOI.
Iroshnikov, P.S.: 1964, *Soviet Astron.* **7**, 566.
Isaacs, J.J., Tessein, J.A., Matthaeus, W.H.: 2015, *J. Geophys. Res. Space Phys.* **120**, 868. DOI.
Jensen, H.J.: 1990, *Phys. Rev. Lett.* **64**, 3103. DOI.
Johnson, J.B.: 1925, *Phys. Rev.* **26**, 71. DOI.
Kadomtsev, B.B., Pogutse, O.P.: 1974, *Sov. Phys. JETP* **38**, 283.
Klein, L.W., Matthaeus, W.H., Roberts, D.A., Goldstein, M.L.: 1992, In: Marsch, E., Schwenn, R. (eds.) *Solar Wind Seven Colloquium*, 197.
Kobayashi, M., Musha, T.: 1982, *IEEE Trans. Biomed. Eng.* **BME-29**, 456. https://api.semanticscholar.org/CorpusID:31743603.
Kraichnan, R.H.: 1965, *Phys. Fluids* **8**, 1385. DOI.
Levitin, D.J., Chordia, P., Menon, V.: 2012, *Proc. Natl. Acad. Sci.* **109**, 3716. DOI.
Machlup, S.: 1981 In: *Sixth International Conference on Noise in Physical Systems*, National Bureau of Standards, Wash. DC, 157.
Magyar, N., Van Doorsselaere, T.: 2022, *Astrophys. J.* **938**, 98. DOI.
Matteini, L., Stansby, D., Horbury, T.S., Chen, C.H.K.: 2018, *Astrophys. J. Lett.* **869**, L32. DOI.
Matthaeus, W.H., Goldstein, M.L.: 1982, *J. Geophys. Res.* **87**, 6011. DOI.
Matthaeus, W.H., Goldstein, M.L.: 1986, *Phys. Rev. Lett.* **57**, 495. DOI.
Matthaeus, W.H., Montgomery, D.: 1980, *Ann. N.Y. Acad. Sci.* **357**, 203. DOI.
Matthaeus, W.H., Breech, B., Dmitruk, P., et al.: 2007, *Astrophys. J. Lett.* **657**, L121. DOI.
Matthaeus, W.H., Chhiber, R., Usmanov, A.V., et al.: 2018 In: *AGU Fall Meeting Abstracts* **2018**, SH54A.
Moncuquet, M., Meyer-Vernet, N., Issautier, K., et al.: 2020, *Astrophys. J. Suppl.* **246**, 44. DOI.
Montgomery, D., Turner, L., Vahala, G.: 1978, *Phys. Fluids* **21**, 757. DOI.
Montgomery, D., Turner, L., Vahala, G.: 1979, *J. Plasma Phys.* **21**, 239. DOI.
Montroll, E.W., Shlesinger, M.F.: 1982, *Proc. Natl. Acad. Sci.* **79**, 3380. DOI.
Mullan, D.J.: 1990, *Astron. Astrophys.* **232**, 520.
Nakagawa, Y., Levine, R.H.: 1974, *Astrophys. J.* **190**, 441. DOI.
Padhye, N.S., Smith, C.W., Matthaeus, W.H.: 2001, *J. Geophys. Res.* **106**, 18635. DOI.
Pecora, F., Yang, Y., Gibson, S., et al.: 2024, *Solar Phys.* **299**, 137. DOI.
Perez, J.C., Chandran, B.D.G.: 2013, *Astrophys. J.* **776**, 124. DOI.
Ponty, Y., Politano, H., Pinton, J.-F.: 2004, *Phys. Rev. Lett.* **92**, 144503. DOI.
Ponty, Y., Mininni, P.D., Montgomery, D.C., et al.: 2005, *Phys. Rev. Lett.* **94**, 164502. DOI.
Rappazzo, A.F., Velli, M., Einaudi, G., Dahlburg, R.B.: 2008, *Astrophys. J.* **677**, 1348. DOI.
Rincon, F.: 2019, *J. Plasma Phys.* **85**, 205850401. DOI.
Ruffolo, D., Matthaeus, W.H., Chhiber, R., et al.: 2020, *Astrophys. J.* **902**, 94. DOI.
Ruiz, M.E., Dasso, S., Matthaeus, W.H., Weygand, J.M.: 2014, *Solar Phys.* **289**, 3917. DOI.
Schottky, W.: 1926, *Phys. Rev.* **28**, 74. DOI.
Schrijver, C.J., Title, A.M.: 2003, *Astrophys. J. Lett.* **597**, L165. DOI.
Servidio, S., Matthaeus, W.H., Shay, M.A., Cassak, P.A., Dmitruk, P.: 2009, *Phys. Rev. Lett.* **102**, 115003. DOI.
Servidio, S., Wan, M., Matthaeus, W.H., Carbone, V.: 2010, *Phys. Fluids* **22**, 125107. DOI.
Shockley, W.: 1957, *Proceedings of the IRE* **45**, 279. DOI.
Taylor, G.I.: 1938, *Proc. Roy. So. London Ser. A* **164**, 476. DOI.
Taylor, J.B.: 1974, *Phys. Rev. Lett.* **33**, 1139. DOI.
Tu, C.Y., Marsch, E.: 1995, *Space Sci. Rev.* **73**, 1. DOI.
Tu, C.Y., Pu, Z.Y., Wei, F.S.: 1984, *J. Geophys. Res.* **89**, 9695. DOI.
Vaĭnshteĭn, S.I., Zel'dovich, Y.B.: 1972, *Sov. Phys. Usp.* **15**, 159. DOI.
Van Der Ziel, A.: 1950, *Physica* **16**, 359. DOI.
Velli, M., Grappin, R., Mangeney, A.: 1989, *Phys. Rev. Lett.* **63**, 1807. DOI.
Verdini, A., Grappin, R., Pinto, R., Velli, M.: 2012, *Astrophys. J. Lett.* **750**, L33. DOI.

Verma, M.K.: 2019, *Energy Transfers in Fluid Flows: Multiscale and Spectral Perspectives*, Cambridge University Press, Cambridge. DOI.
Voss, R.F., Clarke, J.: 1975, *Nature* **258**, 317. DOI.
Woo, R., Armstrong, J.W.: 1979, *J. Geophys. Res.* **84**, 7288. DOI.
Wu, H., Tu, C., Wang, X., He, J., Yang, L.: 2020, *Astrophys. J. Lett.* **904**, L8. DOI.
Wu, H., Tu, C., Wang, X., et al.: 2021, *Astrophys. J.* **912**, 84. DOI.
Zhou, Y., Matthaeus, W.H., Roberts, D.A., Goldstein, M.L.: 1990, *Phys. Rev. Lett.* **64**, 2591. DOI.